Electronic Supplementary Material (ESI) for Journal of Materials Chemistry C.

Supporting Information

An Ultra-High Yield of Spherical K_2NaScF_6:Mn^{4+} Red Phosphor and its Application in Ultra-Wide-Color-Gamut Liquid Crystal Displays

Hong Ming,[a,c] Lili Liu,[a,c] Shengan He,[a,c] Jiaqing Peng,[a,c] Fu Du,[a,c] Junxiang Fu,[a,c] Fengli Yang,[a,c] and Xinyu Ye [a,b,c,]*

[a] *School of Metallurgy and Chemistry Engineering, Jiangxi University of Science and Technology, Ganzhou 341000, P.R. China*

[b] *National Engineering Research Center for Ionic Rare Earth, Ganzhou 341000, P.R. China*

[c] *Key Laboratory of Rare Earth Luminescence Materials and Devices of Jiangxi Province, Ganzhou 341000, P.R. China*

[*] *Corresponding author E-mail: xinyye@yahoo.com*

1. Experimental Section

1.1 Raw materials

All reagents and materials including $KMnO_4$ (A.R.), H_2O_2 (30 wt.%), KHF_2 (99.5%), Sc_2O_3 (99.99%), NaF (99.99%), HF (48 wt.%), Acetic Acid (HAc), acetone (A.R.) and absolute alcohol (A.R.) were used as purchased without further purification. KHF_2, NaF, HF and Sc_2O_3 were supplied by Shanghai Aladdin Biochemical Technology Co., Ltd (China), while other materials (*e.g.*, $KMnO_4$, H_2O_2) were purchased from Guangdong Xilong Scientific Co., Ltd (China). $Cs_4PbBr_6/CsPbBr_3$ nanocomposites (CPB-NCs) and β-Sialon:Eu^{2+} phosphors were supplied by Beijing Nakamura-Yuji Science and Technology Co., Ltd (China), while $CaAlSiN_3$:Eu^{2+} phosphors were purchased from Shandong Yantai SHIELD Advanced Materials Co., Ltd (China). To ensure safety, it is necessary to equip some safeguard requirements (such as patch, glove, fume hoods, *etc.*) during the whole synthesis process.

1.2 Synthesis of K_2NaScF_6:Mn^{4+}

The K_2NaScF_6:Mn^{4+} phosphor was prepared through a simple co-precipitation method according to the schematically illustrated experimental process described in Figure S1. Take K_2NaScF_6:2%Mn^{4+} for example. The pre-set Mn^{4+} source K_2MnF_6 was obtained according to our previous work.[1] 4 mmol Sc_2O_3 (0.5516 g) was weighed and added into a 25 mL Teflon beaker containing 10 ml HF solution, after vigorous magnetic stirring for 30 min, 0.16 mmol K_2MnF_6 (0.0395 g) was put into the above solution and continue stirring for 5 min until completely dissolved. Then, 8 mmol NaF (0.3359 g) and 112 mmol KHF_2 (8.7472 g) were added into the above mixture solution, the mixed solution was kept stirring for further 30 min. After that, the Teflon beaker was quickly put into ice-water bath for 2 h, with the aim of avoiding the valence state change of Mn^{4+} and reducing the volatilization of poisonous HF. The resulting pale-yellow powder product was collected and washed several times with HAc and acetone, then oven-dried at 70 °C for 3 h under a vacuum environment to obtain the final product. As shown in Figure S1a and S1b, the final obtained powders are pale yellow and they emit an intensive red emission light under the irradiation of blue light. In order to investigate the effect of molar ratio of KHF_2 to Sc_2O_3 on the resulting products, a series of K_2NaScF_6:Mn^{4+} samples were obtained by the same procedure according to the synthetic parameters described in Table S1. Besides, different concentrations of Mn^{4+} doped K_2NaScF_6 samples were also synthesized using the same method except for different molar ratios of Sc_2O_3 to K_2MnF_6 (Table S2).

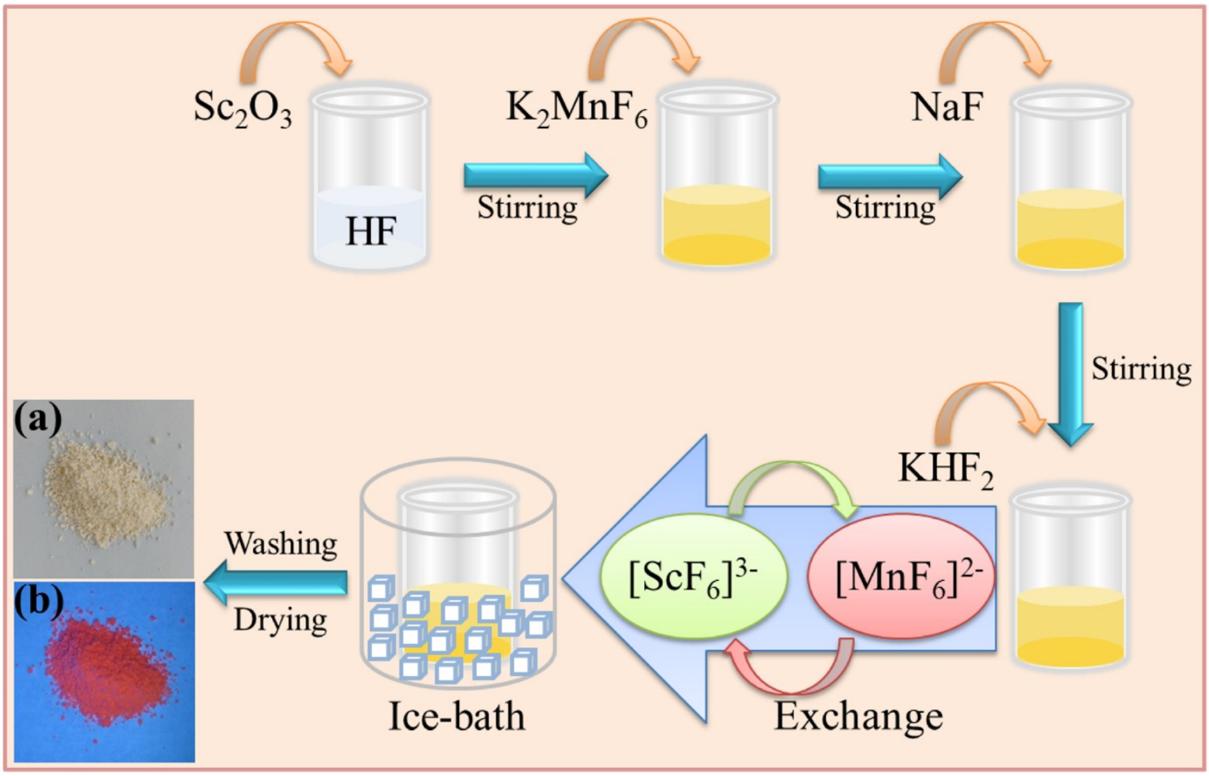

Figure S1. Synthesis schematic diagram for the synthesis of red phosphor K_2NaScF_6:Mn^{4+} from Sc_2O_3, K_2MnF_6, NaF and KHF_2 in HF solution, and digital photographs of the powders under (a) the natural light and (b) the blue light irradiation, respectively.

Table S1. Schemes of different molecular ratios of KHF_2 to Sc_2O_3 for the synthesis of K_2NaScF_6:Mn^{4+} phosphor and nominal doping amount of Mn^{4+} as well as the actual doping amount of Mn^{4+} from ICP-AES test results.

samples	K : Sc (Molar ratio)	nominal doping amount of Mn^{4+} (mol%)	actual doping amount of Mn^{4+} (mol%)
1	6 : 1	3	0.92
2	10 : 1	3	1.45
3	14 : 1	3	2.21
4	18 : 1	3	1.26
5	22 : 1	3	1.06
6	26 : 1	3	0.89
7	30 : 1	3	0.72

Table S2. Schemes of different molecular ratios of Sc_2O_3 to K_2MnF_6 for the synthesis of K_2NaScF_6:Mn^{4+} phosphor and actual doping amount of Mn^{4+} from ICP-AES test results.

samples	Sc : Mn (Molar ratio)	actual doping amount of Mn^{4+} (mol%)
1	100 : 0.5	0.51
2	100 : 1	0.98
3	100 : 2	1.94
4	100 : 4	3.52
5	100 : 6	5.09
6	100 : 8	6.93

1.3 Fabrication of LED devices

The green emitters (β-Sialon:Eu^{2+} phosphors or CPB-NCs), red emitters (as-synthesized K_2NaScF_6:Mn^{4+} phosphors), and blue-emitting InGaN chips (~455 nm, 0.5 W) were used to fabricate pc-WLEDs. These emitters were mixed with epoxy resin thoroughly. The mass ratio of β-Sialon:Eu^{2+}, K_2NaScF_6:Mn^{4+} to epoxy resin is 1:4:10 while the mass ratio of the CPB-NCs, K_2NaScF_6:Mn^{4+} to epoxy resin is 1:3:10. The pc-WLEDs were obtained by coating epoxy resin mixture on the surface of chips and then dried at 150 °C (423 K) for 1 h.

1.4 Characterization

The phase purity of the as-synthesized sample examined by the X-ray powder diffraction (XRD) method on a BRUKER D8 ADVANCED type powder X-ray diffractometer with Cu Kα radiation (λ = 1.5418 Å), performing at 40 kV and 40 mA from 10° to 90° with a scanning step size of 0.02° at 4° min^{-1}. High-angular resolution synchrotron X-ray powder diffraction data were recorded at the BL44B2 beamline of Spring-8 synchrotron radiation facility (Japan) using a constant wavelength of 0.50026 Å and a large Debye-Scherrer camera at room temperature and using a constant wavelength of 0.45 Å. The Rietveld refinement was conducted on the General Structure Analysis System (GSAS) program.[2] Microstructure observations and analyses were performed by using a MIRA3 LMH (TESCAN) scanning electron microscope (SEM) equipped with the energy-dispersive X-ray spectrum (EDS), and a JEOL-2010 transmission electron microscope (TEM). Compositional analyses were verified by an ICP-AES (Optima 8300, PerkinElmer). The XPS spectrum was recorded on a scanning X-ray photoelectron spectroscopy microprobe system (XPS, Phi5000 Versaprobe-Ⅱ, Ulvac-Phi). Diffuse refection spectra (DRS) of the powder samples were measured on a UV-vis-NIR spectrophotometer (Perkin Elmer, Lambda 950) attached to an integral sphere and using barium sulfate as a standard reference. The photoluminescence excitation (PLE), photoluminescence (PL) spectra, quantum yield (QY) and luminescence decay curves were measured at room temperature by an

Edinburgh Instruments FLS980 fluorescence spectrometer, a 450 W xenon lamp was used as the light source. In order to investigate the temperature dependence of the PL properties, the phosphors were placed in a temperature-controlled copper cylinder, and measuring temperature was increased from 300 to 450 K. For low temperature spectra measurement, the phosphors were placed in a closed cycle liquid-helium cooling cryostat, and measurements were performed in the temperature range of 20-300 K. The optical properties, including the luminescent spectrum, luminous efficacy (LE), CRI, CCT, and Commission Internationale de L'Eclairage (CIE) chromaticity coordinates of the LEDs, were measured by a HAAS-2000 (Everfine, China) light and radiation measuring instrument with a photoelectricity test system.

2. Results and discussion

Method for calculating the synthetic yield of K_2NaScF_6:Mn^{4+} phosphor

The procedure (described in part 1.2 of Supporting Information) of K_2NaScF_6:Mn^{4+} samples synthesized with different molar ratio of KHF_2 to Sc_2O_3 (Table S1) was repeated three times. Take the final yield of K_2NaScF_6:Mn^{4+} synthesized with a K/Sc molar ratio of 6 : 1 as an example. The three measured values of synthetic yield for K_2NaScF_6:Mn^{4+} synthesized at a K/Sc molar ratio of 6 : 1 were denoted as M_1, M_2 and M_3, respectively. The final yield value (M) for the K_2NaScF_6:Mn^{4+} sample synthesized with a K/Sc molar ratio of 6 : 1 is determined as follow: $M = \frac{M_1 + M_2 + M_3}{3}$. All samples were weighed after drying at 150 °C for 8 h in a vacuum oven. The final yields of K_2NaScF_6:Mn^{4+} synthesized with different K/Sc molar ratio were determined by the same procedure.

Table S3. Rietveld refinement parameters of conventional X-ray and synchrotron radiation X-ray diffraction profiles of K_2NaScF_6 and K_2NaScF_6:2%Mn^{4+}, respectively. The numbers in parentheses are the estimated standard deviations of the last significant figure.

Formula	K_2NaScF_6	K_2NaScF_6:2%Mn^{4+}
T/K	298	298
symmetry	cubic	cubic
space group	$Fm\bar{3}m$	$Fm\bar{3}m$
a, b, c/Å	8.47418(7)	8.43877(6)
β/degree	90	90
Volume/$Å^3$	608.545(15)	600.950(12)
Z	4	4
2θ-interval/degree	5-120	2-33
Rwp	8.55	5.88
Rp	6.56	4.03
χ^2	1.276	1.096

Table S4. Structural parameters of K_2NaScF_6 as obtained from the Rietveld refinement of conventional X-ray diffraction at room temperature. The numbers in parentheses are the estimated standard deviations of the last significant figure.

Atom	Site	*x*	*y*	*z*	Occ.	U_{iso} (Å^2)
K	8c	0.25	0.25	0.25	1	0.0440(4)
Na	4b	0.50	0.50	0.50	1	0.0330(9)
Sc	4a	0	0	0	1	0.0272(5)
F	24e	0.2341(8)	0	0	1	0.0566(6)

Table S5. Structural parameters of K_2NaScF_6:2%Mn^{4+} as obtained from the combined Rietveld refinement of conventional X-ray and synchrotron radiation X-ray diffraction at room temperature. The numbers in parentheses are the estimated standard deviations of the last significant figure.

Atom	Site	x	y	z	Occ.	U_{iso} (Å^2)
K	8c	0.25	0.25	0.25	0.9957(6)	0.0258(6)
Na	4b	0.50	0.50	0.50	0.9858(7)	0.0084(7)
Sc	4a	0	0	0	0.9816(3)	0.0066(8)
F	24e	0.2339(7)	0	0	1.0000(0)	0.0330(9)
Mn	4a	0	0	0	0.0183(7)	0.0064(3)

Table S6. Standard enthalpy of formation of K_2NaScF_6 and some typical fluorides.

Formula	Standard enthalpy of formation* (ΔH_f^θ, kJ/mol)	Ref.
K_2NaScF_6	-3397.6	[3]
K_2NaGaF_6	-2793.6	[3]
K_2SiF_6	-2807	[4]
Rb_2SiF_6	-2838	[4]
Cs_2SiF_6	-2801	[4]
$(NH_4)_2SiF_6$	-2681	[4]
K_2GeF_6	-2600±8	[4]
K_2NiF_6	-2021±12	[4]

*: The enthalpies of formation ΔH_f^θ were calculated by the same means of the Born-Fajans-Haber thermochemical cycle:[3, 4]

$$\begin{tikzcd}
& xA(c) + M(c) + 3F_2(ss) \arrow[dl, "\Delta H_f^\theta(A_xMF_6)(c)"'] \arrow[dr, "x\Delta H_f^\theta(A^+)(g) + \Delta H_f^\theta([MF_6]^{x-})(g)"] & \\
A_xMF_6(c) \arrow[rr, "U_{POT}(A_xMF_6)"] & & xA^+(g) + [MF_6]^{x-}(g)
\end{tikzcd}$$

where A_xMF_6 represents fluorides (A = K, Na, Rb, Cs or NH_4; $x = 2$, M = Si, Ge, Zr, Ti, Sn or Ni; $x = 3$, M = Al, Ga, In or Sc), (c) represents crystalline state, (g) represents gaseous state, (ss) indicates standard state and the $U_{POT}(A_xMF_6)$ represents lattice energies of fluorides.

Table S7. Solubilities of K_2NaScF_6 and some typical fluorides.

Formula	Experimental solubility values (g/100 ml H_2O), 25 ℃ *	Solubility values found in the literature (g/100 ml H_2O)	Ref.
K_2NaScF_6	0.034		This work
K_3ScF_6	0.210		
K_2TiF_6	1.294		
Na_2TiF_6	7.303		
$(NH_4)_2TiF_6$	29.004		
K_2SiF_6	0.266	0.121 (17 ℃)	[5]
Na_2SiF_6	0.993	0.715 (20 ℃)	[5]
$(NH_4)_2SiF_6$	26.795	21.556 (20 ℃)	[5]
K_3AlF_6	0.292		
Na_3AlF_6	0.913		

*: Experimental solubility values of fluorides in the above table were calculated roughly by using the following procedure. The saturated solution was prepared by adding an excess of a single fluoride (m_1) in the deionized water (100 ml) and maintained at 25 °C for 1 week to reach the equilibrium of solubility. Then, the residue was collected by using the centrifuge reweighed (m_2) after drying at 150 °C for 8 h in a vacuum oven. The dissolved part of the fluoride was not collected by the centrifuge, so its solubility value can be calculated as follow: $S_n = m_1 - m_2$. This procedure was repeated three times for each fluoride and the solubility values were denoted as S_1, S_2 and S_3, respectively. The final solubility value for each fluoride is determined as follow: $S = \frac{S_1 + S_2 + S_3}{3}$. The results are very approach to the reported results.

Table S8. Photoelectric parameters of pc-WLEDs for LCD backlights.

Phosphors		CCT (K)	LE (lm/W)	Color gamut in CIE 1931		Ref.
Green	Red			NSTC (%)	Rec. 2020 (%)	
CCFL				75.0		[6]
RGB LED				105.0		[6]
β-sialon:Eu^{2+}	$CaAlSiN_3$:Eu^{2+}	8620	38 (20 mA)	82.1		[7]
YAG:Ce^{3+}		8000	105 (60 mA)	67.9		[6]
YAG:Ce^{3+}		4950	59	68.3		[7]
β-sialon:Eu^{2+}	K_2SiF_6:Mn^{4+}	8611	94 (120 mA)	85.9		[8]
$CsPbBr_3$	K_2SiF_6:Mn^{4+}			102.0		[9]
β-sialon:Eu^{2+}	K_2NbF_7:Mn^{4+}	11338	94.68 (120 mA)	86.7		[10]
$CsPbBr_3$ QDs	$Na_2WO_2F_4$:Mn^{4+}	12123		107.1		[11]
β-sialon:Eu^{2+}	Cs_2SiF_6:Mn^{4+}	6880	133	84.7		[12]
β-sialon:Eu^{2+}	K_2NaScF_6:Mn^{4+}	5986	67.65 (20 mA)	127.3	95.1	this work
CPB-NCs	K_2NaScF_6:Mn^{4+}	3959	56.29 (20 mA)	129.5	96.7	this work

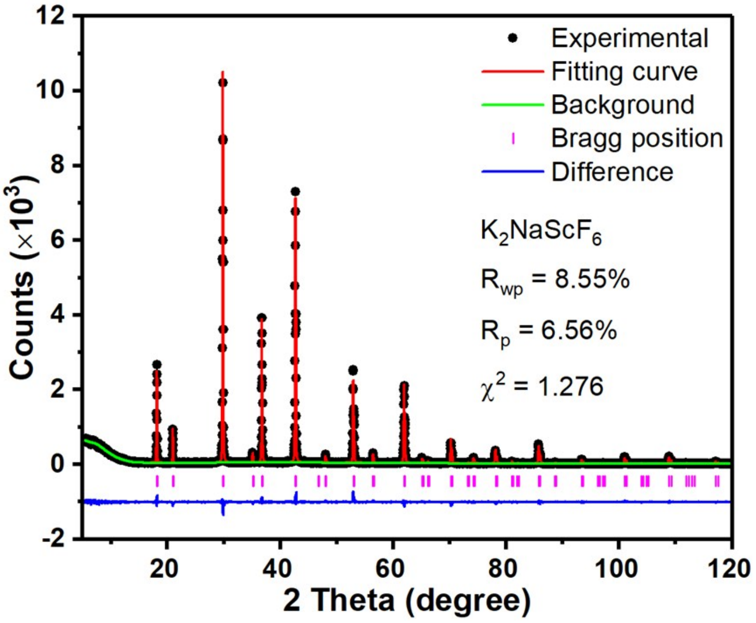

Fig S2. The conventional X-ray Rietveld refinement patterns of K_2NaScF_6. The experimental data for refinement was collected by the Bruker D8 Advanced type powder X-ray diffractometer.

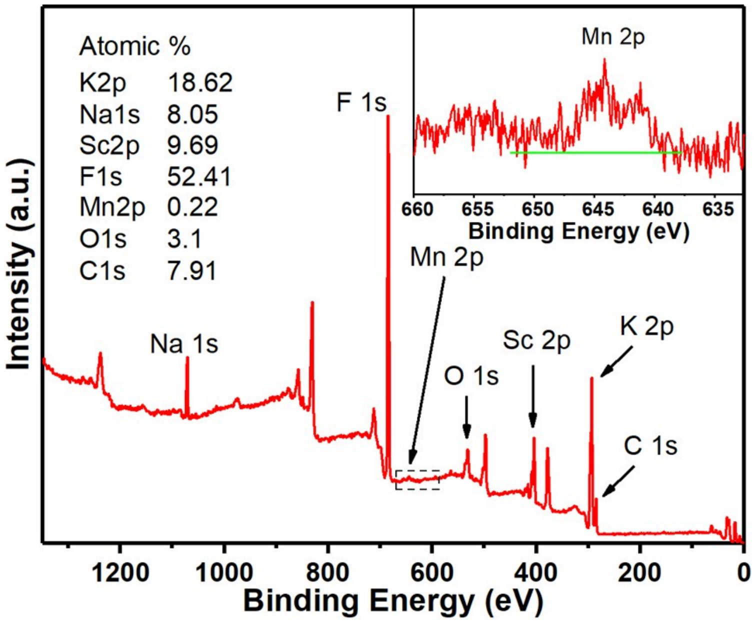

Fig S3. XPS spectrum of K_2NaScF_6:Mn^{4+}. the inset is the magnification of the dot square (Mn^{4+} part).

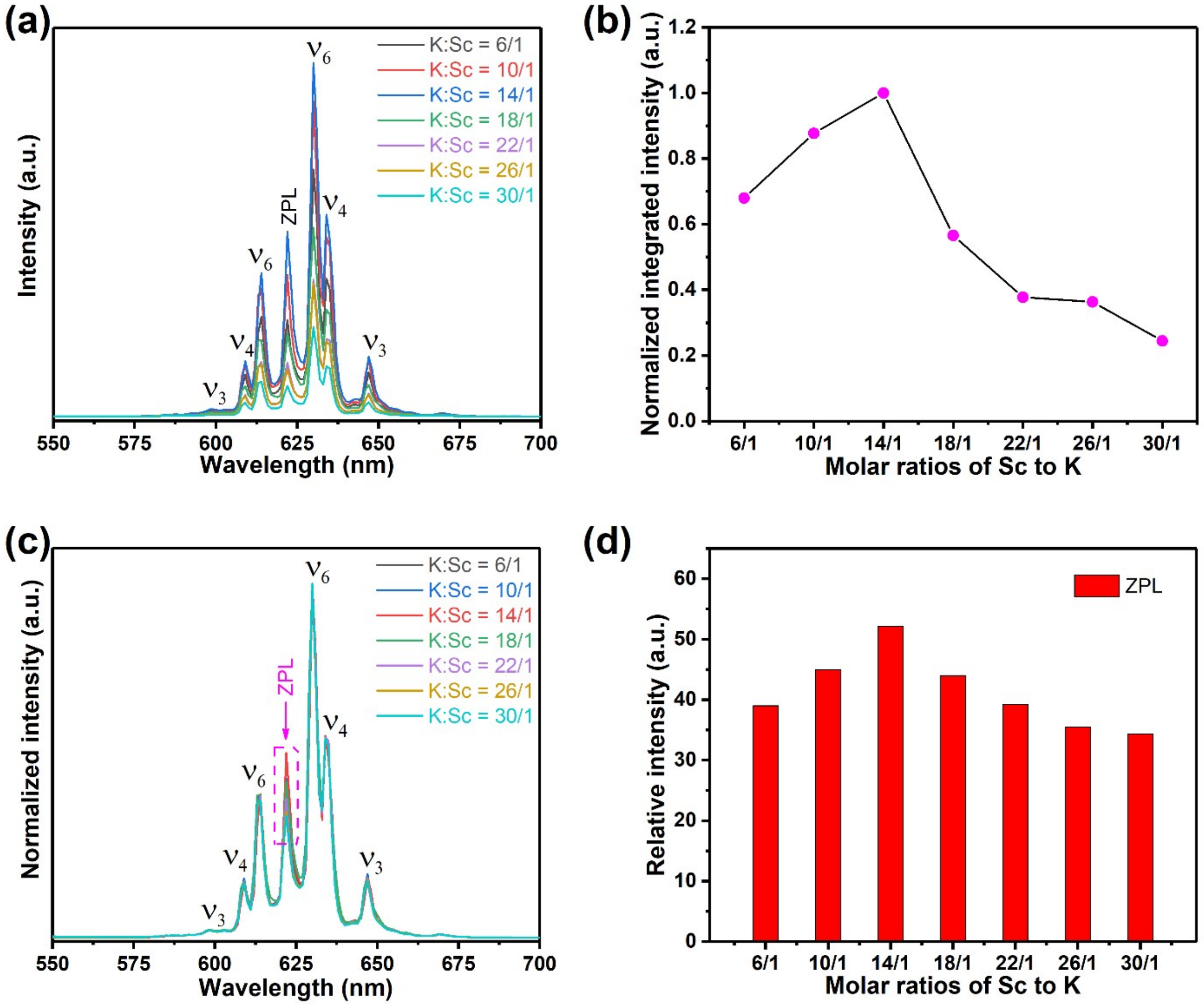

Fig S4. (a) PL spectra (under 468 nm excitation), (b) normalized integrated intensity, (c) normalized PL spectra and (d) the relative ZPL intensity of $K_2NaScF_6:Mn^{4+}$ samples prepared using different molar ratio of K to Sc (K : Sc = 6 : 1, 10 : 1, 14 : 1, 18 : 1, 22 : 1, 26 : 1 and 30 : 1) in HF solution. All synthetic parameters were kept constant except for the examined variables.

In order to check the relationship between PL intensity and the molar ratio of K to Sc, the emission spectra of $K_2NaScF_6:Mn^{4+}$ samples synthesized with different molar ratios of K to Sc (K : Sc = 6 : 1, 10 : 1, 14 : 1, 18 : 1, 22 : 1, 26 : 1 and 30 : 1) are depicted in Figure S4a. Under 468 nm excitation, their PL spectra are almost identical except for the emission intensity. As shown, all the PL spectra consists of seven sharp emission peaks centered at 598, 609, 614, 622, 630, 634, 647 nm, corresponding to the transitions of anti-Stokes $\nu_3(t_{1u})$, $\nu_4(t_{1u})$, $\nu_6(t_{2u})$, zero phonon line (ZPL) and Stokes $\nu_6(t_{2u})$, $\nu_4(t_{1u})$ and $\nu_3(t_{1u})$ vibronic modes of Mn^{4+}:$^2E \rightarrow ^4A_2$, respectively.[13] Meanwhile, It is obviously seen in Figure S4b, the PL intensity of $K_2NaScF_6:Mn^{4+}$ firstly increases with an increasing of the molar ratios of K to Sc and reaches a maximum when the molar ratio of K to Sc is 14 : 1, then monotonously decreases with further increasing the molar ratio of K to Sc. Thus, we believe that the optimal molar ratio of K to Sc for the preparation of $K_2NaScF_6:Mn^{4+}$ is 14 : 1 in the design without considering the synthetic yield. For further understand this phenomenon, the emission spectra of $K_2NaScF_6:Mn^{4+}$ obtained with different molar ratio of K to Sc were normalized and are shown in Figure S4c. The contour of spectra maintains unchanged except the ZPL. Figure S4d presents the change of relative ZPL intensity. The change trend of relative ZPL intensity is the same as the integrated emission intensity of $K_2NaScF_6:Mn^{4+}$ prepared with different molar ratio of K to Sc. It is worth noting that the $K_2NaScF_6:Mn^{4+}$ sample with stronger emission intensity provides a larger emission of ZPL. As a matter of fact, the emission intensity of ZPL is shown to be rigorously determined by the local symmetry of Mn^{4+} surroundings, and the ZPL would be stronger as the lower symmetry of the substituted sites in host lattice.[14] In this system, Mn^{4+} non-equivalently doped into the bigger Sc^{3+} site, and the higher the doping content of Mn^{4+}, the more serious the lattice distortion and the lower the symmetry of the substitution sites. Therefore, despite the fact that the molar ratio of K_2MnF_6 to Sc_2O_3 is fixed in our experiment, it can be reasonably concluded that the actual doping amount of Mn^{4+} is different for the $K_2NaScF_6:Mn^{4+}$ samples synthesized with different molar ratios of K to Sc. To confirm whether the actual Mn^{4+} doping amount of $K_2NaScF_6:Mn^{4+}$ samples show similar dependence, $K_2NaScF_6:Mn^{4+}$ samples synthesized with different molar ratios of K to Sc were further studied by using the Inductively Coupled Plasma-Atomic Emission Spectrometry (ICP-AES) technology, as shown in Table S1. It is found that the dependence of the actual Mn^{4+} doping amount of $K_2NaScF_6:Mn^{4+}$ samples on the molar ratios of K to Sc is perfectly consistent with that of the ZPL (Figure S4d) as well as the PL intensity (Figure S4b), suggesting that the dependence of PL intensity of $K_2NaScF_6:Mn^{4+}$ samples on the molar ratios of K to Sc is inherently due to the changing amount of activator, *i.e.*, Mn^{4+} ion, controlled by the amount of KHF_2. The analytical results show that an appropriate increase in the amount of KHF_2 into the reaction system may enhance the effective Mn^{4+} doping amount of

K_2NaScF_6:Mn^{4+} phosphor. However, with further increasing the input amount of KHF_2, the effective Mn^{4+} doping amount tends to decrease gradually. A possible reason for this phenomenon is that excessive K^+ ions badly exacerbated the charge imbalance when the trivalent Sc^{3+} ions were substituted by the tetravalent Mn^{4+} ions.[15]

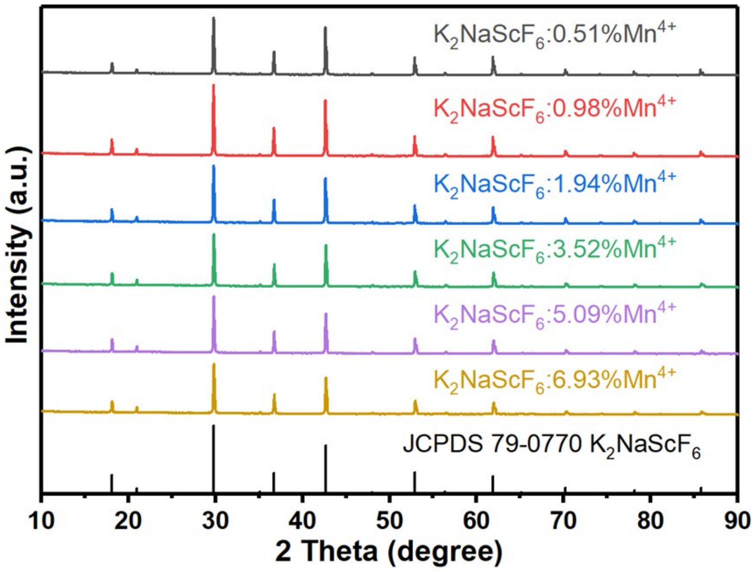

Fig S5. XRD patterns of K_2NaScF_6:Mn^{4+}samples doped with different content of Mn^{4+}.

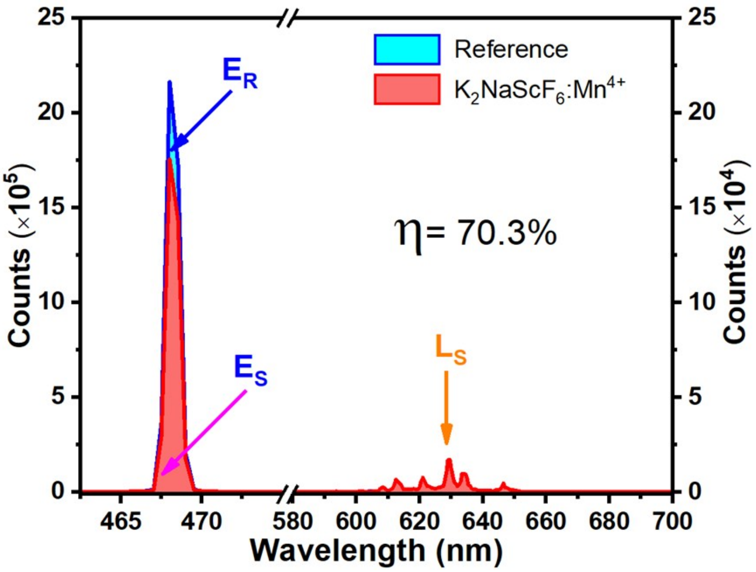

Fig S6. PL spectra (under 468 nm excitation) of K_2NaScF_6:Mn^{4+} and reference sample measured using an integrating sphere for quantum yield.

The QY of K_2NaScF_6:Mn^{4+} phosphor was measured by using an integrating sphere coated with barium sulfate at room-temperature attached to the spectrophotometer. The IQY (symbolized as η_{int}) can be calculated by using the following equation:[10]

$$\eta_{int} = \frac{\int L_s}{\int E_R - \int E_S}$$

where L_S represents the emission spectrum of the studied K_2NaScF_6:Mn^{4+} phosphor, and E_S and E_R are the excitation spectra of the excitation light used for exciting the product and without the product in the integrating sphere, respectively.

The AE of the sample, ε_{abs}, can be calculated by the following expression:

$$\varepsilon_{abs} = \frac{E_R - E_S}{E_R}$$

thereupon, the EQY (symbolized as η_{ext}) can be determined by the following equation:

$$\eta_{ext} = \varepsilon_{abs} \times \eta_{int}$$

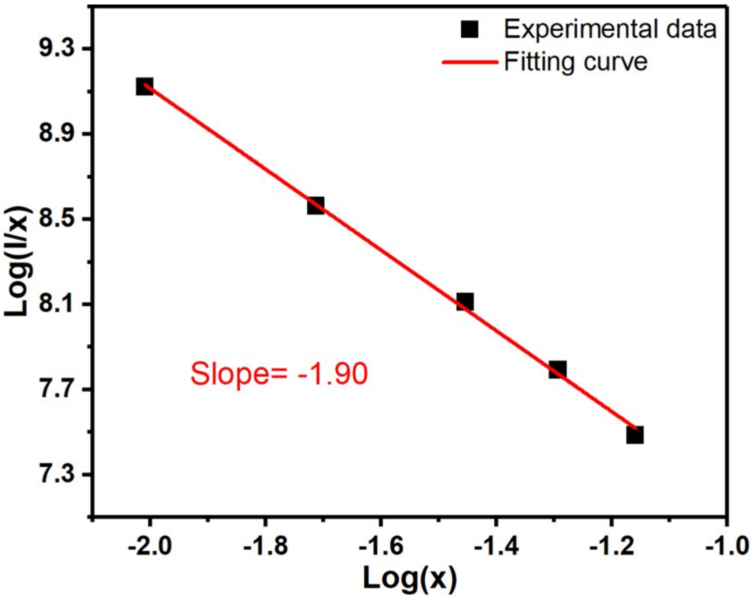

Fig S7. The relationship plot between log(I/x) versus log(x) for the $K_2NaScF_6:Mn^{4+}$ phosphor. (Note: x represents the doping content of Mn^{4+}.)

To obtain a better understanding of the concentration quenching characteristics of $K_2NaScF_6:Mn^{4+}$ phosphor, the critical distance R_c proposed by Blasse between the adjacent Mn^{4+} ions was estimated according to the following equation:[16, 17]

$$R_c \approx 2 \times \left(\frac{3V}{4\pi x_c N}\right)^{1/3}$$

in which x_c represents the critical concentration of Mn^{4+} in the matrix, V is the unit cell volume and N represents the number of available sites that the activator can substitute in the host lattice. For the K_2NaScF_6 matrix, $V = 608.545$ Å^3, $N = 4$ and the critical concentration x_c is 1.94 mol%. So, the critical distance (R_c) for energy transfer is determined to be 24.65 Å. It is well known that the exchange interaction can only occur when the R_c is less than 5 Å. While, the calculated R_c is much bigger than 5 Å, implying that there is almost no exchange interaction in the energy transfer between Mn^{4+} ions. Hence, the non-radiative energy transfer mechanism for Mn^{4+} ions in K_2NaScF_6 matrix is considered to be the multipolar interaction. On the basis of the Dexter theory, the related type of the multipolar interaction can be determined by using the following equation:[18, 19]

$$\frac{I}{x} = K\left[1 + \beta(x)^{\frac{\theta}{3}}\right]^{-1}$$

where I and x represent the integrated emission intensity and the concentration of activator that is no less than the x_c, respectively. K and β are constants. The θ equals to 6, 8, and 10, corresponding to the dipole-dipole (d-d), dipole-quadrupole (d-q), and quadrupole-quadrupole (q-q) interaction, respectively. The above equation can be approximately deformalized as below:

$$\log\left(\frac{I}{x}\right) = -\frac{\theta}{3}\log x + A$$

as shown in Figure S7, the relationship of log(I/x) versus log(x) appears to be linear, possessing a slope ($-\theta/3$) of -1.90. The corresponding θ is calculated to be 5.70 and close to 6. Thus, the concentration quenching of Mn^{4+} in K_2NaScF_6 host lattice is mainly because of the dipole-dipole (d-d) interaction.

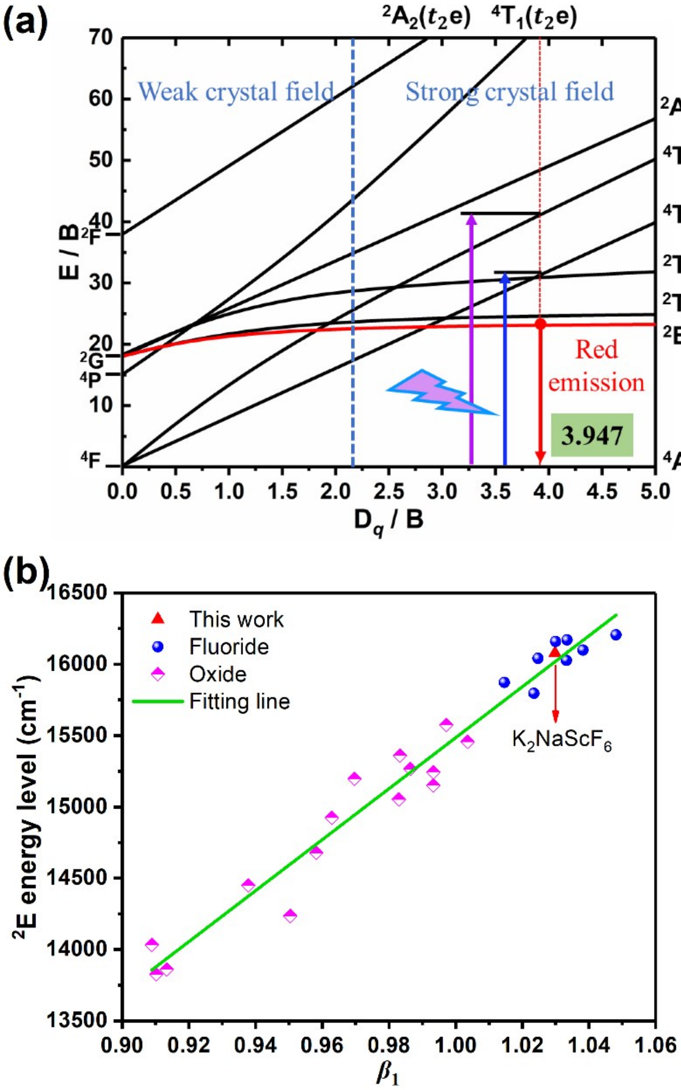

Fig S8. (a) Tanabe-Sugano energy-level diagram of Mn^{4+} in an octahedral crystal field. (b) Empirical linear relationship between the Mn^{4+}:^2E_g energy level and the nephelauxetic ratio β_1.

The effect of an octahedral environment on the energy levels of Mn^{4+} $3d^3$ can be well illustrated by the Tanabe-Sugano diagram, as show in Figure S8a. The crystal field strength D_q for Mn^{4+} ions in the K_2NaScF_6 matrix can be determined by the peak energy of Mn^{4+}:$^4A_2 \rightarrow {}^4T_2$ (21368 cm^{-1}) according to the following expression:[20]

$$D_q = \frac{E(^4A_2 \rightarrow {}^4T_2)}{10}$$

The values of D_q is estimated to be ~2137 cm^{-1}. On the basis of the difference of peak energy (5880 cm^{-1}) between Mn^{4+}: $^4A_2 \rightarrow {}^4T_1$ (27248 cm^{-1}) and $^4A_2 \rightarrow {}^4T_2$ (21368 cm^{-1}), the Racah parameter B can be determined as below:[20]

$$\frac{D_q}{B} = \frac{15(x-8)}{(x^2-10x)}$$

here, the definition of the parameter x is as follows:[20]

$$x = \frac{E(^4A_2 \rightarrow {}^4T_1) - E(^4A_2 \rightarrow {}^4T_2)}{D_q}$$

The Racah parameter C is determined using the following formula:[20]

$$\frac{E(^2E \rightarrow {}^4A_2)}{B} = \frac{3.05C}{B} + 7.9 - \frac{1.8B}{D_q}$$

The estimated values of B and C for the K_2NaScF_6:Mn^{4+} phosphor are ~541 cm^{-1} and ~3950 cm^{-1}, respectively, and consequently, the D_q/B equals to ~3.947, suggesting that Mn^{4+} ions in K_2NaScF_6 host lattice suffer from a strong crystal field strength (Figure S8a).

As is well-known, the ^2E energy level of Mn^{4+} is almost unaffected by the crystal field while its position differs from host to host, which results in different emission wavelength of Mn^{4+}:$^2E \rightarrow {}^4A_2$ (16077 cm^{-1}). The main cause of this change in energies of the transition (Mn^{4+}:$^2E \rightarrow {}^4A_2$) is the nephelauxetic effect depending on the covalency of the metal-ligand chemical bond. To evaluate the covalent effect of Mn^{4+} in the K_2NaScF_6 matrix, the nephelauxetic ratio β_1 established by Brik et al. is calculated using the following equation:[21]

$$\beta_1 = \sqrt{(\frac{B}{B_0})^2 + (\frac{C}{C_0})^2}$$

where B_0 (1160 cm^{-1}) and C_0 (4303 cm^{-1}) are the Racah parameters of Mn^{4+} ions (free state) in a crystal, respectively. For Mn^{4+}-doped K_2NaScF_6, the β_1 is determined to be ~1.0298, and the data point (β_1, E), as depicted in Figure S8b, follows the empirical line established by Brik and Srivastava well and approaches other points of fluorides.[21]

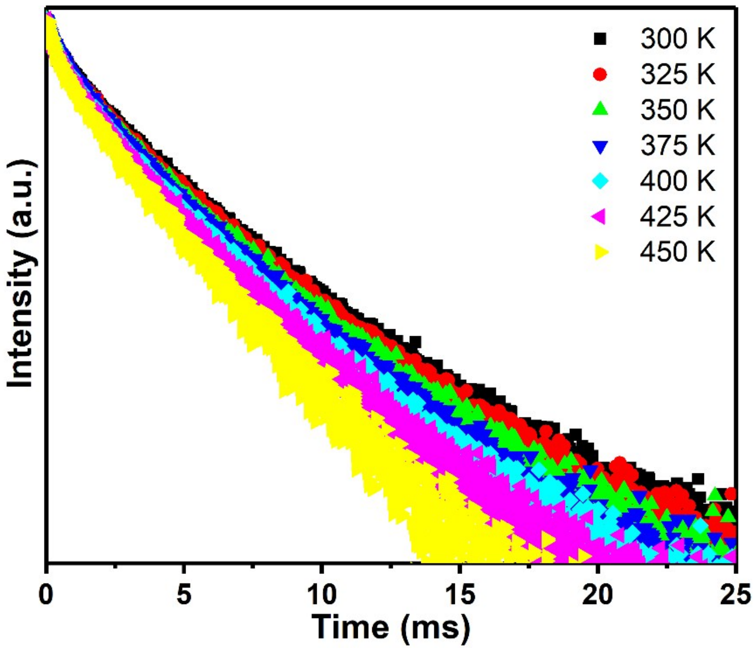

Fig S9. The luminescence decay curves of $K_2NaScF_6:Mn^{4+}$ phosphor during the heating processes.

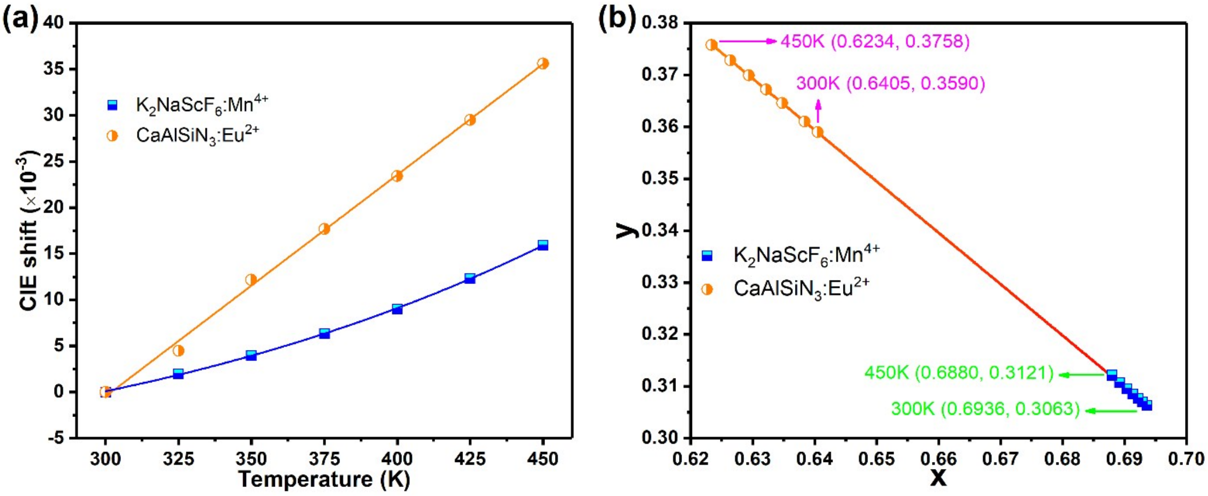

Fig S10. CIE chromaticity shifts (a) and CIE color coordinates (b) of $K_2NaScF_6:Mn^{4+}$ and $CaAlSiN_3:Eu^{2+}$ in the temperature region from 300 to 450 K.

The color stability was quantifiably evaluated by using the chromaticity shift (ΔE). The chromaticity shift (ΔE) of phosphors in the temperature range of 300-450 K can be calculated according to the following equation:[22]

$$\Delta E=\sqrt{(u'_t-u'_0)^2+(v'_t-v'_0)^2+(w'_t-w'_0)^2}$$

where $u'=4x/(3-2x+12y)$, $v'=9y/(3-2x+12y)$, and $w'=1-u'-v'$. u' and v' are the chromaticity coordinates in $u'v'$ uniform color space, x and y are the chromaticity coordinates in CIE 1931 color space, 0 and t are the chromaticity shift at 300 K and a given temperature, respectively. As presented in Figure S10a, as the increase of temperature, the chromaticity shifts of $K_2NaScF_6:Mn^{4+}$ and $CaAlSiN_3:Eu^{2+}$ (purchased from Yantai SHIELD Advanced Materials Co., Ltd.) both increases gradually, while the chromaticity shift of $CaAlSiN_3:Eu^{2+}$ increases faster. At 450 K (175 °C), $CaAlSiN_3:Eu^{2+}$ shows the chromaticity shift of ~ 36×10^{-3}, which is more than twice that of $K_2NaScF_6:Mn^{4+}$ (~16×10^{-3}). Moreover, Figure S10b displays the temperature-dependent CIE color coordinates of $K_2NaScF_6:Mn^{4+}$ and $CaAlSiN_3:Eu^{2+}$ phosphors in detail. With the temperature increases from 300 K to 450 K, the CIE color coordinate of $K_2NaScF_6:Mn^{4+}$ shifts from (0.6936, 0.3063) to (0.6880, 0.3121), and its luminescent color is still in the red region. By contrast, the CIE color coordinate of $CaAlSiN_3:Eu^{2+}$ shifts from the red region (0.6405, 0.3589) to the orange region (0.6234, 0.3758). In summary, the $K_2NaScF_6:Mn^{4+}$ phosphor shows a preferable color stability with a slight chromaticity shift within the red region, which is mainly ascribed to the broadening and negligible shifting of the red line peaks of Mn^{4+}.[13] These results further demonstrate that $K_2NaScF_6:Mn^{4+}$ is a potential red phosphor as the efficient red supplement for high-quality pc-WLEDs.

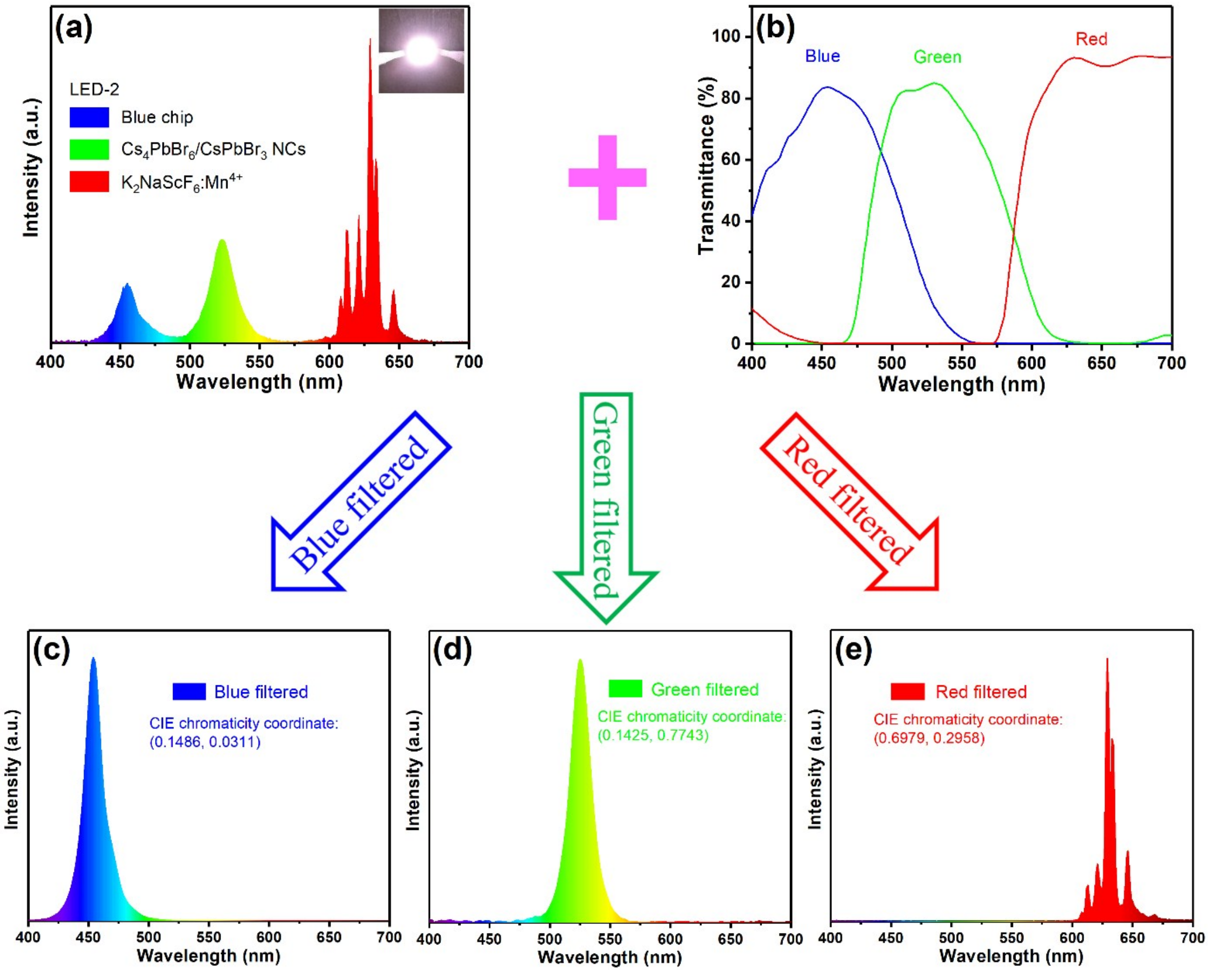

Fig S11. (a) Electroluminescence spectra of LED-2. (b) Transmittance spectrum of the commercial red, green, and blue color filters. (c), (d) and (e) are the corresponding EL spectra after filtering.

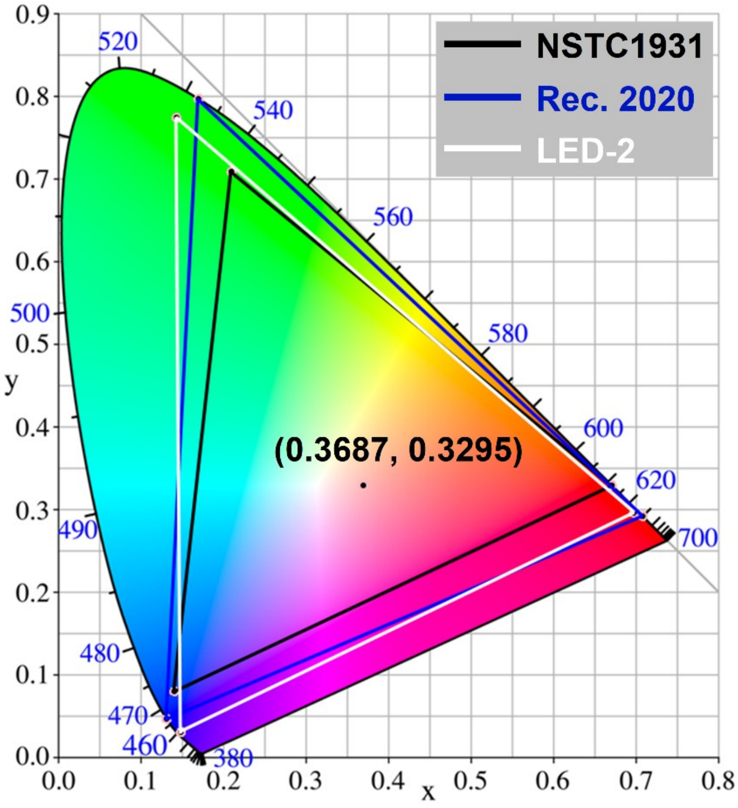

Fig S12. The CIE 1931 color coordinates corresponding to the constructed LED-2 (white triangles), the NTSC standard (black triangles) and the Rec. 2020 standard (blue triangles).

References:

1. Ming, H.; Liu, S.; Liu, L.; Peng, J.; Fu, J.; Du, F.; Ye, X., Highly Regular, Uniform $K_3ScF_6:Mn^{4+}$ Phosphors: Facile Synthesis, Microstructures, Photoluminescence Properties, and Application in Light-Emitting Diode Devices. *ACS Appl. Mater. Interfaces* **2018,** 10, (23), 19783-19795.

2. Larson, A. C.; Von Dreele, R. B., Gsas. *General Structure Analysis System. LANSCE, MS-H805, Los Alamos, New Mexico* **1994**.

3. Marx, V., Lattice energy and heat of formation of elpasolite type K_2NaScF_6 and K_2NaGaF_6. *Phys. Status Solidi B* **2000,** 220, (2), 805-810.

4. Jenkins, H. D. B.; Pratt, K. F., Lattice Energies and Thermochemistry of Hexahalometallate(iv) Complexes, A_2MX_6, Which Possess the Antifluorite Structure. In Advances in Inorganic Chemistry and Radiochemistry (Vol. 22, pp. 1-111). Academic Press. **1979**.

5. Frayret, J.; Castetbon, A.; Trouve, G.; Potin-Gautier, M., Solubility of $(NH_4)_2SiF_6$, K_2SiF_6 and Na_2SiF_6 in acidic solutions. *Chem. Phys. Lett.* **2006,** 427, (4-6), 356-364.

6. Oh, J. H.; Kang, H.; Ko, M.; Do, Y. R., Analysis of wide color gamut of green/red bilayered freestanding phosphor film-capped white LEDs for LCD backlight. *Opt. Express* **2015,** 23, (15), A791-A804.

7. Xie, R. J.; Hirosaki, N.; Takeda, T., Wide Color Gamut Backlight for Liquid Crystal Displays Using Three-Band Phosphor-Converted White Light-Emitting Diodes. *Appl.Phys. Express* **2009,** 2, (2), 022401.

8. Wang, L.; Wang, X.; Kohsei, T.; Yoshimura, K.; Izumi, M.; Hirosaki, N.; Xie, R. J., Highly efficient narrow-band green and red phosphors enabling wider color-gamut LED backlight for more brilliant displays. *Opt. Express* **2015,** 23, (22), 28707-28717.

9. Zhang, X.; Wang, H. C.; Tang, A. C.; Lin, S. Y.; Tong, H. C.; Chen, C. Y.; Lee, Y. C.; Tsai, T. L.; Liu, R. S., Robust and Stable Narrow-Band Green Emitter: An Option for Advanced Wide-Color-Gamut Backlight Display. *Chem. Mater.* **2016,** 28, (23), 8493-8497.

10. Lin, H.; Hu, T.; Huang, Q.; Cheng, Y.; Wang, B.; Xu, J.; Wang, J.; Wang, Y., Non-Rare-Earth $K_2XF_7:Mn^{4+}$ (X = Ta, Nb): A Highly-Efficient Narrow-Band Red Phosphor Enabling the Application in Wide-Color-Gamut LCD. *Laser Photonics Rev.* **2017,** 11, (6), 1700148.

11. Hu, T.; Lin, H.; Cheng, Y.; Huang, Q.; Xu, J.; Gao, Y.; Wang, J.; Wang, Y., A highly-distorted octahedron with a C_{2v} group symmetry inducing an ultra-intense zero phonon line in Mn^{4+}-activated oxyfluoride $Na_2WO_2F_4$. *J. Mater. Chem. C* **2017,** 5, (40), 10524-10532.

12. Liu, Y.; Zhou, Z.; Huang, L.; Brik, M. G.; Si, S.; Lin, L.; Xuan, T.; Liang, H.; Qiu, J.; Wang, J., High-performance and moisture-resistant red-emitting $Cs_2SiF_6:Mn^{4+}$ for high-brightness LED backlighting. *J. Mater. Chem. C* **2019,** 7, (8), 2401-2407.

13. Deng, T. T.; Song, E. H.; Sun, J.; Wang, L. Y.; Deng, Y.; Ye, S.; Wang, J.; Zhang, Q. Y., The design and preparation of the thermally stable, Mn^{4+} ion activated, narrow band, red emitting fluoride $Na_3GaF_6:Mn^{4+}$ for warm WLED applications. *J. Mater. Chem. C* **2017,** 5, (11), 2910-2918.

14. Wang, L. Y.; Song, E. H.; Deng, T. T.; Zhou, Y. Y.; Liao, Z. F.; Zhao, W. R.; Zhou, B.; Zhang, Q. Y., Luminescence properties and warm white LED application of a ternary-alkaline fluoride red phosphor $K_2NaAlF_6:Mn^{4+}$. *Dalton Trans.* **2017,** 46, (30), 9925-9933.

15. Cheng, H. M.; Song, Y.; Liu, G. X.; Li, D.; Dong, X. T.; Wang, J. X.; Yu, W. S., Hydrothermal synthesis of narrow-band red emitting $K_2NaAlF_6:Mn^{4+}$ phosphor for warm-white LED applications. *Rsc Adv.* **2017,** 7, (72), 45834-45842.

16. Zhu, M.; Pan, Y.; Huang, Y.; Lian, H.; Lin, J., Designed synthesis, morphology evolution and enhanced photoluminescence of a highly efficient red dodec-fluoride phosphor, $Li_3Na_3Ga_2F_{12}:Mn^{4+}$, for warm WLEDs. *J. Mater. Chem. C* **2018,** 6, (3), 491-499.

17. Blasse, G., Luminescence of inorganic solids: from isolated centres to concentrated systems. *Prog. Solid State Chem.* **1988,** 18, (2), 79-171.

18. Dexter, D. L., A Theory of Sensitized Luminescence in Solids. *J. Chem. Phys.* **1953,** 21, (5), 836-850.

19. Lv, W.; Jia, Y.; Zhao, Q.; Jiao, M.; Shao, B.; Lü, W.; You, H., Crystal structure and luminescence properties of $Ca_8Mg_3Al_2Si_7O_{28}:Eu^{2+}$ for WLEDs. *Adv. Opt. Mater.* **2014,** 2, (2), 183-188.

20. Brik, M. G.; Camardello, S. J.; Srivastava, A. M.; Avram, N. M.; Suchocki, A., Spin-Forbidden Transitions in the Spectra of Transition Metal Ions and Nephelauxetic Effect. *ECS J. Solid State Sci. Technol.* **2015,** 5, (1), R3067-R3077.

21. Brik, M. G.; Camardello, S. J.; Srivastava, A. M., Influence of Covalency on the Mn^{4+} $^2E_g \rightarrow ^4A_{2g}$ Emission Energy in Crystals. *ECS J. Solid State Sci. Technol.* **2014,** 4, (3), R39-R43.

22. Huang, L.; Zhu, Y.; Zhang, X.; Zou, R.; Pan, F.; Wang, J.; Wu, M., HF-Free Hydrothermal Route for Synthesis of Highly Efficient Narrow-Band Red Emitting Phosphor $K_2Si_{1-x}F_6:xMn^{4+}$ for Warm White Light-Emitting Diodes. *Chem. Mater.* **2016,** 28, (5), 1495-1502.